

Distilling Knowledge into Quantum Vision Transformers for Biomedical Image Classification

Thomas Boucher[✉] and Evangelos B. Mazomenos[✉]

UCL Hawkes Institute, Department of Medical Physics and Biomedical Engineering,
University College London, London, United Kingdom.
{thomas.boucher.23, e.mazomenos}@ucl.ac.uk

Abstract. Quantum vision transformers (QViTs) build on vision transformers (ViTs) by replacing linear layers within the self-attention mechanism with parameterised quantum neural networks (QNNs), harnessing quantum mechanical properties to improve feature representation. This hybrid approach aims to achieve superior performance, with significantly reduced model complexity as a result of the enriched feature representation, requiring fewer parameters. This paper proposes a novel QViT model for biomedical image classification and investigates its performance against comparable ViTs across eight diverse datasets, encompassing various modalities and classification tasks. We assess models trained from scratch and those pre-trained using knowledge distillation (KD) from high-quality teacher models. Our findings demonstrate that QViTs outperform comparable ViTs with average ROC AUC (0.863 vs 0.846) and accuracy (0.710 vs 0.687) when trained from scratch, and even compete with state-of-the-art classical models in multiple tasks, whilst being significantly more efficient (89% reduction in GFLOPs and 99.99% in parameter number). Additionally, we find that QViTs and ViTs respond equally well to KD, with QViT pre-training performance scaling with model complexity. This is the first investigation into the efficacy of deploying QViTs with KD for computer-aided diagnosis. Our results highlight the enormous potential of quantum machine learning (QML) in biomedical image analysis.¹

Keywords: Biomedical Image Classification · Quantum Vision Transformers · Knowledge Distillation.

1 Introduction

Vision transformers (ViTs) [5] have emerged as a transformative architecture in computer vision. By treating images as sequences of patches, and leveraging self-attention to capture long-range dependencies and intricate patterns within image data, ViTs have demonstrated exceptional performance for biomedical classification tasks, often surpassing convolutional neural networks (CNNs) [16].

In parallel, quantum machine learning (QML) has recently witnessed significant advancements, with a surge of applications in biomedical image analysis

¹ Code and models are available at <https://github.com/surgical-vision/QViT-KD>.

[20]. Quantum neural networks (QNNs) exploit the properties of quantum mechanics to represent information in ways that are fundamentally more complex than classical systems. Unlike classical neural networks that operate in Euclidean spaces, QNNs leverage Hilbert spaces, the natural domain for quantum states. Hilbert spaces facilitate richer representations due to quantum phenomena absent in Euclidean space. This enhanced representational power enables QNNs to capture intricate data patterns with greater parameter efficiency, leading to more effective machine learning, particularly supervised learning [9].

Quantum vision transformers (QViTs) represent a hybrid classical-quantum approach combining the strengths of ViTs with the rich feature representation of QNNs. In QViTs the linear layers within the attention mechanism are replaced with QNNs to produce quantum self-attention (QSA). This QSA mechanism harnesses quantum mechanical properties within Hilbert spaces to enhance feature representation. Whilst research into QViTs is still in its nascent stages, QViT architectures have recently shown great promise in classification tasks, even competing with classical models with vastly more parameters [3], highlighting their potential for high-performance parameter-efficient QML. Subsequently, techniques to further refine their efficiency and performance are crucial.

Knowledge distillation (KD) [11] offers a compelling direction. KD transfers knowledge from a large, complex teacher model to a smaller, simpler student model, intending to improve the student’s performance. Having proven successful in enhancing small ViTs [21], KD presents a particularly relevant approach

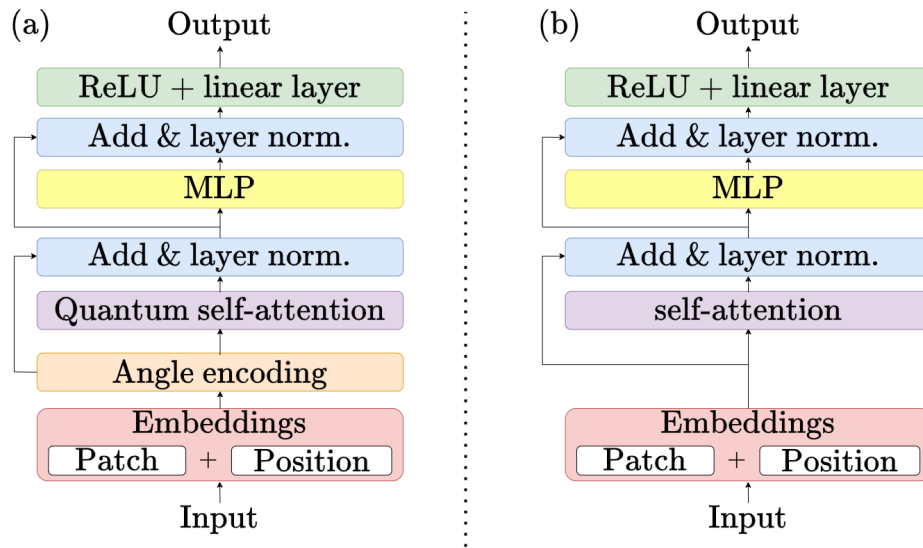


Fig. 1. (a) The QViT architecture, utilising quantum self-attention following angle-encoding in place of classical self-attention, (b) the respective ViT architecture.

for QViTs. It allows the rich knowledge captured in parameter-heavy classical teacher models to be leveraged to guide the training of parameter-efficient hybrid student models. Such investigations into the efficacy of KD pre-training for QViTs for biomedical image classification is unexplored in the literature.

We address this and evaluate the effect of KD pre-training for QViTs in biomedical image analysis with a comprehensive investigation. We systematically compare the performance of QViTs against classical ViTs of comparable complexity for biomedical image classification across eight diverse datasets. These datasets encompass eight distinct imaging modalities, a variety of binary and multi-class classification tasks, and an ordinal regression task. We evaluate the performance of models trained both from scratch and with KD pre-training from a high-quality classical teacher model, under a range of training conditions.

We make the following contributions: (1) we present the first investigation into the efficacy of pre-training QViTs with KD for biomedical image classification; (2) we demonstrate the potential for our novel QViT architecture to outperform equivalent ViTs, visualised in Fig. 1 (a) and (b) respectively, improving average ROC AUC and accuracy 2.01% and 3.35% respectively across eight diverse datasets; (3) we show that QViTs with a very low number of parameters are capable of outperforming state-of-the-art (SOTA) classical models, both when learning from scratch and with KD pre-training, illustrating the ability for QML to provide high-performance parameter-efficient classifiers.

2 Primer: Quantum Networks

Quantum networks are comprised of *qubits*, which represent a continuous superposition of quantum states. These states are parametrised by complex probability amplitudes of unit norm:

$$|\psi\rangle = \alpha|0\rangle + \beta|1\rangle = \begin{bmatrix} \alpha \\ \beta \end{bmatrix} \in \mathbb{H}, \quad \alpha, \beta \in \mathbb{C}, \quad |\alpha|^2 + |\beta|^2 = 1, \quad (1)$$

where \mathbb{H} is a Hilbert space. This allows qubits to occupy an infinite number of states, enhancing their representational power compared to a bit, which is binary. Quantum states are transformed by unitary operations, which are also essential for encoding classical data onto quantum networks via a *quantum feature map* $x \in \mathbb{R} \rightarrow |\psi(x)\rangle \in \mathbb{H}$. For an n -qubit network initialised in a state $|0\rangle^n = \bigotimes_{i=1}^n |0\rangle$, this encoding is a unitary transformation $U_\psi(x)|0\rangle^n = |\psi(x)\rangle$. We use *angle encoding*, which encodes n classical bits onto n qubits. For $x \in \mathbb{R}^n$:

$$U_\psi = \bigotimes_{i=1}^n U_{x_i}, \quad U_{x_i} := \begin{bmatrix} \cos(x_i/2) & -\sin(x_i/2) \\ \sin(x_i/2) & \cos(x_i/2) \end{bmatrix} \quad (2)$$

This is chosen for its time efficiency and high performance in quantum classifiers [7]. This encoded state can then be transformed by further parametrised unitary operations $U(\Theta)|\psi(x)\rangle = |\psi'(x)\rangle$, $U(\Theta) \in \text{U}(n)$. A specific sequence of parametrised unitary operations is an *ansatz*, which is typically designed to act

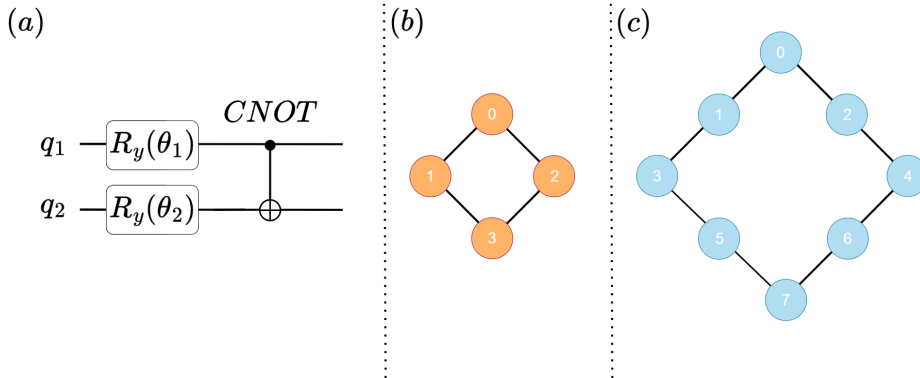


Fig. 2. (a) The ansatz we use, applied to qubit pairs (q_1, q_2) , (b) the four-qubit and (c) the eight qubit QNNs structure we use, with paired qubits connected by lines.

on qubit pairs. We use a low parameter ansatz, visualised in Fig. 2(a), shown to be effective, with angle encoding, for classification tasks [12]. This ansatz applies a parametrised unitary operation $R_y(\theta_i)$ to each qubit for $i = 1, 2$, followed by a controlled-NOT (CNOT):

$$R_y(\theta_i) := \begin{bmatrix} \cos(\theta_i/2) & -\sin(\theta_i/2) \\ \sin(\theta_i/2) & \cos(\theta_i/2) \end{bmatrix}, \quad \text{CNOT} := \begin{bmatrix} 1 & 0 & 0 & 0 \\ 0 & 1 & 0 & 0 \\ 0 & 0 & 0 & 1 \\ 0 & 0 & 1 & 0 \end{bmatrix}, \quad (3)$$

where CNOT, defined by $\text{CNOT}(|q_1\rangle \otimes |q_2\rangle) := |q_1\rangle \otimes |(q_1 \oplus q_2) \bmod 2\rangle$, *entangles* the two qubits, creating a joint state which is essential for quantum algorithms to achieve computational advantages over classical methods [13].

To extract classical information from the network, a unitary operation Z is used to measure the expectation value $\langle Z \rangle$ of each qubit, defined by:

$$\langle Z \rangle := \langle \psi | Z | \psi \rangle = [\alpha \ \beta] \begin{bmatrix} 1 & 0 \\ 0 & -1 \end{bmatrix} \begin{bmatrix} \alpha \\ \beta \end{bmatrix} = |\alpha|^2 - |\beta|^2 \in \mathbb{R}. \quad (4)$$

Performing this measurement for each qubit produces a vector $y \in \mathbb{R}^n$.

3 Methods

We evaluate the classification performance of QViTs by comparing them to ViTs with equivalent parameter counts; the standard practice when assessing the utility of QNNs [10]. We use the QViT architecture of [2], where QNNs replace the linear projection layers for key, query, and value to produce a QSA mechanism. The ViT architecture uses linear layers that match the dimensionality of these QNNs. For both modelspatch embeddings are extracted using convolutions and

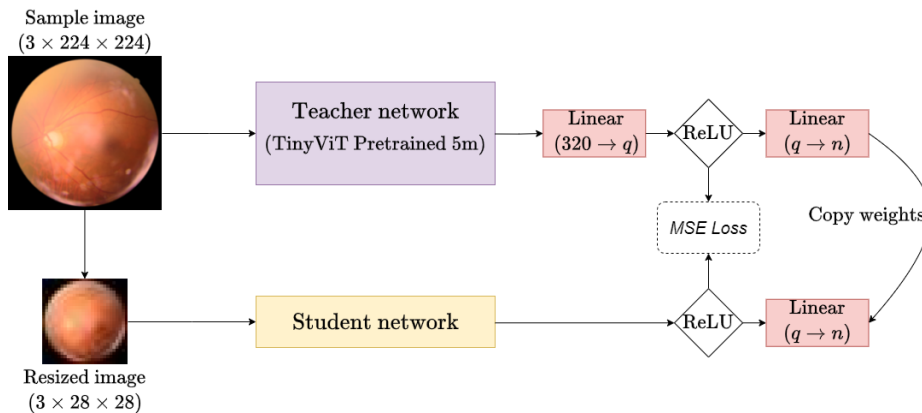


Fig. 3. The KD architecture for a sample image from RetinaMNIST with a 28×28 input student network, where q is the number of qubits, n is number of target classes. The student is optimised to minimise the MSE loss between the teacher’s and student’s intermediate logits. Following KD training, the teacher’s final linear layer weights are copied to the student’s final layer. For 224×224 inputs, the resizing step is skipped.

combined with positional embeddings. These embeddings are processed through the attention mechanism, followed by a multilayer perceptron (MLP), before passing through a rectified linear unit (ReLU) and final linear layer for classification. Layernorm and residual connections are used for training stability.

We compare the models for varying image and patch size, for single-head and multi-head attention, and for varying number of qubits. The specific qubit configurations, visualised in Fig. 2 (b) and (c), are chosen to be deployable to IBM and Rigetti quantum processors. For each task, we assess performance both when learning from scratch and with KD pre-training. For training, we followed the procedure in [22], using an Adam optimiser with an initial learning rate of 1×10^{-3} for 100 epochs, which decreased by a factor of ten after 50 and 75 epochs, and batch size of 32. For KD, we use the 5M-parameter TinyViT model [21] as the teacher network, itself pre-trained via KD on ImageNet. Pretrained ViTs have been shown to perform well when fine-tuned for biomedical classification tasks [8], and its small size relative to other, larger models makes it more suitable for KD with our small models [4]. We fine-tune TinyViT independently on each dataset to create a task-specific teacher. We align both the penultimate logit representation and the final layer of the teacher and student networks. We modify TinyViT’s classification head by replacing the original linear layer with two linear layers: the first mapping to the number of qubits, and the second mapping to the number of output classes, with a ReLU activation function in between. The logits following the ReLU in the teacher network serve as targets for the equivalent logits in the student network. For KD pre-training, we used an Adam optimiser

with a learning rate of 1×10^{-3} for 50 epochs, a batch size of 32, and mean squared error (MSE) loss, which is effective for classification via KD [14].

To leverage the shared final linear layer structure between teacher and student, we initialised the student’s final layer with the teacher’s weights. This weight transfer is justified by the KD process, which optimises the student’s penultimate layer to mirror the teacher’s, ensuring weight compatibility. We use this method of KD over direct logit KD on the final layer as we found it produced better results for both models, increasing ViT and QViT classification accuracy by 9.31% and 14.1% respectively. This KD architecture is visualised in Fig. 3.

Following KD pre-training, the student models are trained end-to-end as classifiers on each dataset independently. All development was completed on a single NVIDIA GeForce RTX 4090 GPU, utilising PennyLane [1] with PyTorch for quantum circuit simulation and automatic differentiation.

4 Results

We evaluate our models across eight different biomedical classification tasks:

MedMNIST [22]: A large-scale collection of biomedical images, including 12 datasets of 2D images, all with defined train/validation/test splits and corresponding classification labels. We select seven of the datasets for time efficiency, encompassing seven modalities and a range of binary and multi-label classification tasks, and an ordinal regression task.

OASIS [17]: A dataset of brain MRI scans divided into four classes based on Alzheimer’s progression. Axial slices were used as input, with only slices between the 100th and 160th slice considered for each patient. We use a subset of the full dataset for a better balance between the four classes and for time efficiency.

All models were trained on each dataset using 28×28 RGB images with 2×2 patches and 224×224 RGB images with 16×16 patches, for both single-head and multi-head attention. Training results from scratch and with KD pretraining are in Table 1 and Table 2 respectively, with the latter also containing the results for the fine-tuned TinyViT teacher model. Results for multi-head attention are presented in both tables due to superior performance for both ViTs and QViTs.

5 Discussion

Our analysis demonstrates that QViTs compete with and can even outperform comparable ViTs. When considering the average performance across all metrics and datasets, QViT was superior to ViT, achieving both higher average ROC AUC (0.863 vs 0.846) and average accuracy (0.710 vs 0.687). When assessing performance with KD pre-training, QViT-KD and ViT-KD perform comparably in both average ROC AUC (0.849 vs 0.855) and average accuracy (0.696 vs 0.699). Moreover, QViT demonstrated exceptionally strong performance in some tasks, achieving results comparable to SOTA models. For example, all four QViT instances performed competitively with ResNet18 and ResNet50 on the

Table 1. Performance comparison of four qubit QViT and ViT with two-headed attention trained from scratch. Top score in each metric for each dataset is in bold.

Methods	BreastMNIST		RetinaMNIST		PneumoniaMNIST		DermaMNIST	
	AUC	ACC	AUC	ACC	AUC	ACC	AUC	ACC
ViT_28	0.733	0.821	0.690	0.468	0.931	0.846	0.863	0.694
ViT_224	0.709	0.744	0.696	0.528	0.931	0.849	0.870	0.691
QViT_28	0.788	0.801	0.748	0.565	0.904	0.862	0.857	0.695
QViT_224	0.735	0.763	0.683	0.525	0.944	0.856	0.862	0.696

Methods	BloodMNIST		OrganCMNIST		PathMNIST		OASIS	
	AUC	ACC	AUC	ACC	AUC	ACC	AUC	ACC
ViT_28	0.979	0.844	0.912	0.574	0.932	0.686	0.822	0.701
ViT_224	0.976	0.835	0.938	0.627	0.944	0.687	0.603	0.400
QViT_28	0.968	0.812	0.923	0.618	0.934	0.684	0.812	0.693
QViT_224	0.969	0.815	0.947	0.633	0.933	0.650	0.785	0.678

Table 2. Performance comparison of four qubit QViT and ViT with two-headed attention pre-trained with KD from a high-performance teacher (TinyViT).

Methods	BreastMNIST		RetinaMNIST		PneumoniaMNIST		DermaMNIST	
	AUC	ACC	AUC	ACC	AUC	ACC	AUC	ACC
ViT-KD_28	0.770	0.756	0.701	0.518	0.935	0.824	0.865	0.696
ViT-KD_224	0.681	0.731	0.708	0.488	0.938	0.825	0.857	0.685
QViT-KD_28	0.636	0.750	0.744	0.535	0.938	0.864	0.849	0.693
QViT-KD_224	0.714	0.763	0.720	0.510	0.943	0.840	0.860	0.701
TinyViT	0.900	0.904	0.790	0.618	0.988	0.886	0.933	0.823

Methods	BloodMNIST		OrganCMNIST		PathMNIST		OASIS	
	AUC	ACC	AUC	ACC	AUC	ACC	AUC	ACC
ViT-KD_28	0.976	0.839	0.914	0.613	0.942	0.709	0.810	0.693
ViT-KD_224	0.981	0.863	0.906	0.555	0.942	0.682	0.749	0.652
QViT-KD_28	0.972	0.824	0.928	0.612	0.921	0.660	0.764	0.641
QViT-KD_224	0.971	0.815	0.917	0.613	0.939	0.712	0.763	0.656
TinyViT	0.999	0.989	0.997	0.956	0.990	0.889	0.983	0.965

PneumoniaMNIST dataset, with QViT_28 and QViT-KD_28 surpassing these models on RetinaMNIST [22]. Notably, on RetinaMNIST, QViT_28 outperformed 13/14 SOTA classifiers in terms of accuracy, including CNN and ViT based methods, and all but one MedMamba model [23]. This competitive performance on RetinaMNIST was achieved with a negligible reduction (0.88%) in classification accuracy, but with a 89% reduction in GFLOPs and a 99.99% reduction in parameters compared to the higher performing MedMamba model. Additionally, QViTs exhibit a greater benefit from attention head scaling than ViTs, with QViTs’ two-head attention yielding ROC AUC and accuracy gains of 3.16% and 6.10% over single-head, beating ViTs’ gains of 0.15% and 2.95%.

Due to the cost of using real quantum computers, we used simulated quantum networks. These simulations accurately represent the network behavior, but are severely limited by $\mathcal{O}(2^n)$ computational complexity for n qubits. This computational cost restricts the size of the QNNs we can simulate. Consequently, our QViTs were limited to a low parameter count of around 1K for the (28) models and 4K for the (224) models. Whilst this is sufficient to assess the advantage of using QSA, it likely hindered the capacity to benefit from KD [4], explaining the underperformance of KD-pretrained models. This is supported by the comparative performance of QViT-KD_28 and QViT-KD_224 models. The larger QViT-KD_224 model, with four times the parameters of QViT-KD_28 due to larger patch embeddings, demonstrated superior performance in average ROC AUC (0.853 vs 0.844) and accuracy (0.701 vs 0.697). Furthermore, the performance gap between freshly-trained and KD pre-trained models reduced with increased parameter size. QViT-KD_28 performed 2.65% worse than QViT_28 in both average ROC AUC and accuracy, while QViT-KD_224 showed a smaller performance reduction of 0.47% in ROC AUC and 0.14% in accuracy compared to QViT_224; a disparity reduction of 82.26% and 94.72% respectively. To further investigate this, we trained QViT_224 and QViT-KD_224 with eight qubits instead of four, increasing parameter number to 8K. In this case, QViT-KD_224 outperformed QViT_224 for both ROC AUC (0.881 vs 0.857) and accuracy (0.763 vs 0.720), and showed an increase in these metrics over the four qubit QViT-KD_224 of 3.28% and 8.84% respectively. Moreover, this eight-qubit QViT-KD_224 outperforms the equivalent ViT-KD_224 in average ROC AUC (0.881 vs 0.867) and accuracy (0.763 vs 0.749), and is competitive with the SOTA on BloodMNIST, performing just 0.40% and 4.78% worse than the top model for ROC AUC and accuracy. We expect similar performance behaviour for QViT_28 and QViT-KD_28 with eight qubit configurations.

Due to simulation computational complexity, training of QViT is around $8\times$ the time for ViT for four qubit configurations. Recent advancements in distributed quantum computing have demonstrated the feasibility of integrating numerous quantum processing modules into a network [15], reinforcing the practical feasibility of the QViT distributed architecture on real quantum hardware, without the need for classical simulation. Our QNN simulations also exclude interference effects, a decision supported by the groundbreaking Willow [6] and Majorana 1 [18,19] quantum chips, which have shown that large scale, interference-mitigating qubit networks will become available in the near future.

Our results clearly demonstrate the potential advantages of hybrid classical-quantum neural networks for biomedical image classification, with the capability to surpass classical-only models with a fraction of the parameters. QViTs demonstrated strong performance across multiple tasks, and the underlying principles of QViTs suggest the possibility of effective generalisation to a wide range of tasks involving complex biomedical image data. This, together with ongoing developments, underscores the potential advantages of QViTs and the likelihood for widespread deployment and clinical application within years.

References

1. Bergholm, V., et al.: PennyLane: Automatic differentiation of hybrid quantum-classical computations. arXiv preprint arXiv:1811.04968 [quant-ph] (2022)
2. Cara, M.C., Dahale, G.R., Dong, Z., Forestano, R.T., Gleyzer, S., Justice, D., Kong, K., Magorsch, T., Matchev, K.T., Matcheva, K., Unlu, E.B.: Quantum vision transformers for quark-gluon classification. *Axioms* (2024)
3. Cherrat, E.A., Kerenidis, I., Mathur, N., Landman, J., Strahm, M., Li, Y.Y.: Quantum Vision Transformers. *Quantum* **8**, 1265 (2024)
4. Cho, J.H., Hariharan, B.: On the efficacy of knowledge distillation. In: Proceedings of the IEEE/CVF ICCV. pp. 4794–4802 (2019)
5. Dosovitskiy, A., Beyer, L., Kolesnikov, A., Weissenborn, D., Zhai, X., Unterthiner, T., Dehghani, M., Minderer, M., Heigold, G., Gelly, S., Uszkoreit, J., Houlsby, N.: An image is worth 16x16 words: Transformers for image recognition at scale. arXiv preprint arXiv:2010.11929 [cs.CV] (2021)
6. Google Quantum AI and Collaborators: Quantum error correction below the surface code threshold. *Nature* (2024)
7. Grant, E., Benedetti, M., Cao, S., Hallam, A., Lockhart, J., Stojevic, V., Green, A.G., Severini, S.: Hierarchical quantum classifiers. *NPJ Quantum Inf* **4**(1), 65 (2018)
8. Halder, A., Gharami, S., Sadhu, P., Singh, P.K., Woźniak, M., Ijaz, M.F.: Implementing vision transformer for classifying 2d biomedical images. *Sci Rep* **14**(1), 12567 (2024)
9. Havlíček, V., Córcoles, A.D., Temme, K., Harrow, A.W., Kandala, A., Chow, J.M., Gambetta, J.M.: Supervised learning with quantum-enhanced feature spaces. *Nature* **567**(7747), 209–212 (2019)
10. Herrmann, N., Arya, D., Doherty, M.W., Mingare, A., Pillay, J.C., Preis, F., Prestel, S.: Quantum utility—definition and assessment of a practical quantum advantage. In: 2023 IEEE QSW. pp. 162–174. IEEE (2023)
11. Hinton, G., Vinyals, O., Dean, J.: Distilling the knowledge in a neural network. arXiv preprint arXiv:1503.02531 [stat.ML] (2015)
12. Hur, T., Kim, L., Park, D.K.: Quantum convolutional neural network for classical data classification. *Quant Mach Intell* **4**(1), 3 (2022)
13. Jozsa, R., Linden, N.: On the role of entanglement in quantum-computational speed-up. *Proc. R. Soc. Lond., Ser. A, Math. Phys. Eng. Sci.* **459**(2036), 2011–2032 (2003)
14. Kim, T., Oh, J., Kim, N., Cho, S., Yun, S.Y.: Comparing kullback-leibler divergence and mean squared error loss in knowledge distillation. pp. 2628–2635. *IJCAI* (2021)
15. Main, D., Drmota, P., Nadlinger, D., Ainley, E., Agrawal, A., Nichol, B., Srinivas, R., Araneda, G., Lucas, D.: Distributed quantum computing across an optical network link. *Nature* pp. 1–6 (2025)
16. Manzari, O.N., Ahmadabadi, H., Kashiani, H., Shokouhi, S.B., Ayatollahi, A.: Medvit: a robust vision transformer for generalized medical image classification. *Comput. Biol. Med* **157**, 106791 (2023)
17. Marcus, D.S., Wang, T.H., Parker, J., Csernansky, J.G., Morris, J.C., Buckner, R.L.: Open access series of imaging studies (oasis): cross-sectional mri data in young, middle aged, nondemented, and demented older adults. *JoCN* **19**(9), 1498–1507 (2007)
18. Microsoft Azure Quantum: Interferometric single-shot parity measurement in inas-hybrid devices. *Nature* **638**(8051), 651–655 (2025)

19. Microsoft Quantum: Roadmap to fault tolerant quantum computation using topological qubit arrays. arXiv preprint arXiv:2502.12252 [quant-ph] (2025)
20. Wei, L., Liu, H., Xu, J., Shi, L., Shan, Z., Zhao, B., Gao, Y.: Quantum machine learning in medical image analysis: A survey. *Neurocomputing* **525**, 42–53 (2023)
21. Wu, K., Zhang, J., Peng, H., Liu, M., Xiao, B., Fu, J., Yuan, L.: Tinyvit: Fast pretraining distillation for small vision transformers. In: *ECCV*. pp. 68–85 (2022)
22. Yang, J., Shi, R., Wei, D., Liu, Z., Zhao, L., Ke, B., Pfister, H., Ni, B.: Medmnist v2- a large-scale lightweight benchmark for 2d and 3d biomedical image classification. *Sci. Data* **10**(1), 41 (2023)
23. Yue, Y., Li, Z.: Medmamba: Vision mamba for medical image classification. arXiv preprint arXiv:2403.03849 [eess.IV] (2024)